ReaxFF Reactive Force Field for Molecular Dynamics Simulations of Hydrocarbon Oxidation

Kimberly Chenoweth, Adri C. T. van Duin, and William A. Goddard, III*

Materials and Process Simulation Center (139-74), California Institute of Technology, Pasadena, California 91125

Received: October 10, 2007; In Final Form: November 27, 2007

To investigate the initial chemical events associated with high-temperature gas-phase oxidation of hydrocarbons, we have expanded the ReaxFF reactive force field training set to include additional transition states and chemical reactivity of systems relevant to these reactions and optimized the force field parameters against a quantum mechanics (QM)-based training set. To validate the ReaxFF potential obtained after parameter optimization, we performed a range of NVT–MD simulations on various hydrocarbon/O_2 systems. From simulations on methane/O_2, *o*-xylene/O_2, propene/O_2, and benzene/O_2 mixtures, we found that ReaxFF obtains the correct reactivity trend (propene > *o*-xylene > methane > benzene), following the trend in the C–H bond strength in these hydrocarbons. We also tracked in detail the reactions during a complete oxidation of isolated methane, propene, and *o*-xylene to a $CO/CO_2/H_2O$ mixture and found that the pathways predicted by ReaxFF are in agreement with chemical intuition and our QM results. We observed that the predominant initiation reaction for oxidation of methane, propene, and *o*-xylene under fuel lean conditions involved hydrogen abstraction of the methyl hydrogen by molecular oxygen forming hydroperoxyl and hydrocarbon radical species. While under fuel rich conditions with a mixture of these hydrocarbons, we observed different chemistry compared with the oxidation of isolated hydrocarbons including a change in the type of initiation reactions, which involved both decomposition of the hydrocarbon or attack by other radicals in the system. Since ReaxFF is capable of simulating complicated reaction pathways without any preconditioning, we believe that atomistic modeling with ReaxFF provides a useful method for determining the initial events of oxidation of hydrocarbons under extreme conditions and can enhance existing combustion models.

1. Introduction

A great deal of progress has been made over the last 20 years in elucidating the reaction mechanisms and kinetics for gas-phase oxidation of hydrocarbons,[1–16] where the chemistry is dominated by bimolecular and unimolecular processes. Much less progress has been made in establishing the fundamental reaction mechanisms and kinetic parameters for high pressure and condensed phase oxidations, where it is difficult to disentangle the various fundamental steps from the final product distributions obtained experimentally. Similarly, the theoretical and computational approaches that are contributing so much to the understanding of bimolecular and unimolecular processes are most difficult to apply to condensed phases where one might need to deal with thousands of atoms for periods of nanoseconds or longer, which is far too long for molecular dynamics (MD) based on ab initio quantum mechanics (QM). In order to enable the computational study of such large systems for such long periods, we have developed the ReaxFF reactive force field which retains nearly the accuracy of QM but allows MD for computational costs nearly as low as for simple force fields. Applications using ReaxFF for studying reactive processes have been reported for many systems including organic reactions,[17] reactions of energetic materials under extreme conductions,[18,19] decomposition of improvised explosive devices,[20] thermal decomposition of polymers,[21] BiMoOx heterogeneous catalysts,[22] fuel cells,[23] crack propagation in silicon crystals,[24] dissociation of H_2 on Pt surfaces,[25] storage of H_2 in Mg

nanoclusters,[26] catalytic formation of carbon nanotubes,[27] and tribology of metal–metal oxide interfaces.[28] A reliable ReaxFF force field for hydrocarbon oxidation is essential in studying the interface chemistry and reactions on metals, metal oxides, and other catalyst systems. In this paper, we use ReaxFF to investigate the initial steps of oxidation of O_2 with several organic systems. This illustrates how ReaxFF may be applied to complex oxidations. The studies here include only modest sized systems and modest periods; however, ReaxFF calculations of reactive processes have already been reported on systems with 1 000 000 atoms. Thus, with suitable computational facilities, one can consider such studies on problems ranging from thermal decomposition of the precursors to petroleum to shock induced oxidations of organics.

Pervasive use of hydrocarbon fuels has led to extensive experimental and theoretical research in order to gain a detailed understanding of the processes involved in combustion.[1–9] The combustion reaction is initiated by thermal decomposition and abstraction of hydrogen atoms from smaller hydrocarbon molecules resulting in the formation of radicals.[1–3,6,8,9] These radicals can then react to form smaller olefins and partially oxidized hydrocarbon species. While combustion of saturated hydrocarbons is highly efficient, combustion of unsaturated hydrocarbons such as benzene is less efficient yielding polyaromatic hydrocarbons and large amounts of soot.[4,9] A detailed knowledge of the elementary chemical kinetics and thermochemistry of the reactions involved in the process is necessary for current kinetic models of combustion.

Simple alkanes have been extensively studied using kinetic modeling and combustion experiments, but for larger alkanes

* To whom correspondence should be addressed: E-mail: wag@wag.caltech.edu.

MD Simulations of Hydrocarbon Oxidation

J. Phys. Chem. A, Vol. 112, No. 5, 2008 **1041**

such as octane, only the most important isomers (e.g., *iso*-octane and *n*-octane) have been studied.[9] As the size of the molecule increases, the number of elementary reactions needed to describe the complete oxidation of these systems increases as well, and modeling becomes computationally expensive. In order to reduce the computational burden, a study was performed by Qin et al.[10] to determine if the parameter sets obtained from optimization of smaller-hydrocarbon mechanisms could be used directly. Through a detailed reaction mechanism optimization for propane combustion, it was shown that experimental results cannot be replicated by simply optimizing the rate parameters of C_3 elementary reactions while keeping the rate parameters from smaller hydrocarbons ($C_{<3}$) fixed at values obtained through optimization against $C_{<3}$ combustion data.[10] In general, combustion tends to be very complex and reduced kinetic schemes[9,11−15] have been developed to allow simulation of complicated combustion devices but do not provide atomistic description of the initiation processes. Determination of the various intermediates that are formed during the pre-ignition period could provide important information for pollution control, since even minor species can play a vital role in the formation of undesirable byproducts and harmful emissions.[16] In addition, there is a substantial need for detailed reaction information regarding the impact of promoters and inhibitors as well as contaminants on the combustion chemistry of hydrocarbons at various pressures and temperatures.[9]

Current kinetic modeling methods do not provide an atomistic description of the critical initial reactive events associated with hydrocarbon oxidation. Although single event microkinetic models being used in the area of cracking[29−31] allow for the simulation of a few reactions in a complicated reaction pathway, it is difficult to form a complete description of the processes since all reactions are classified by reaction classes and the kinetics can only be simulated for each individual step. For this reason, an accurate, computationally feasible, atomistic method to describe the chemical reactivity could enhance existing combustion models. Quantum mechanical (QM) methods can provide accurate barriers and reaction energies for individual reactions but these methods are too computationally expensive to provide a detailed, dynamical description of complex oxidation reactions and the effects of temperature and pressure on the reaction path. We have demonstrated that a QM-derived ReaxFF reactive force field[17] can be used to study complicated chemical processes over long time scales for large systems such as elucidating the chemical events associated with thermal decomposition of nitramine RDX,[18,19] triacetonetriperoxide,[20] and poly(dimethyl)siloxane polymer.[21] Here, we present the development of an accurate reactive force field for carrying out molecular dynamics (MD) simulations for the investigation of the chemical processes associated with hydrocarbon oxidation. The ReaxFF reactive force field was developed to allow bond dissociation and formation during dynamic simulations. Since the ReaxFF force field parameters are derived solely from QM, it can be directly applied to novel systems that may not have been extensively studied experimentally. ReaxFF does not require pre-defined reactive sites or reaction pathways. Therefore, results from a ReaxFF-based MD simulation provide an unbiased representation of the pre- and post-ignition oxidation chemistry.

Here, we describe an expansion of the ReaxFF reactive force field for hydrocarbons[9] by adding QM data for transition states and chemical reactivity of systems relevant to hydrocarbon oxidation to the original hydrocarbon training set. We present results from NVT−MD simulations of the gas-phase high-temperature oxidation of individual hydrocarbons including methane, propene, *o*-xylene, and benzene. In addition, a simulation was performed with a system containing a mixture of the various hydrocarbons and oxygen. A detailed chemical analysis of the simulations was performed to determine initial reactive events and simulation time required for initiation, as well as final product distributions. These simulations demonstrate the ability of ReaxFF to describe the chemical events associated with combustion and should provide an accurate tool for analyzing pre-ignition, ignition, and quenching chemistry.

2. Computational Methods

2.1. ReaxFF Reactive Force Field Method. ReaxFF is a general bond-order-dependent force field that provides accurate descriptions of bond breaking and bond formation (e.g., see refs 17−28). The main difference between traditional unreactive force fields and ReaxFF is that in ReaxFF the connectivity is determined by bond orders calculated from interatomic distances that are updated every MD step. This allows for bonds to break and form during the simulation. In order to account for nonbonded interactions such as van der Waals and Coulomb interactions for a system with changing connectivity, these interactions are calculated between every pair of atoms, irrespective of connectivity, and any excessive close-range nonbonded interactions are avoided by inclusion of a shielding term. In addition, ReaxFF accounts for polarization effects by using a geometry-dependent charge calculation scheme. A full description of all ReaxFF potential functions can be found in Supporting Information.

The force field parameters were determined by combining the original hydrocarbon training set[17] with the QM data for transition states and reaction energies for systems relevant to hydrocarbon oxidation. The optimization of the parameters was carried out via a single-parameter search optimization[32] to minimize the following sum of squares:

$$\text{Error} = \sum_{i=1}^{n}\left[\frac{(x_{i,\text{QM}} - x_{i,\text{ReaxFF}})}{\sigma}\right]^2 \qquad (1)$$

where x_{QM} is the QM value, x_{ReaxFF} is the ReaxFF calculated value, and σ is the accuracy specified in the training set. The full set of ReaxFF potential functions and force field parameters have been supplied in Supporting Information.

2.2. Quantum Mechanical Calculations. ReaxFF force field parameter values were obtained by optimization against a training set that contained data from QM calculations. The QM calculations were performed using the B3LYP[33] hybrid DFT functional and the Pople 6-311G** basis set[34] as implemented in Jaguar (Version 6.5).[35] The B3LYP flavor of DFT has been validated to yield an average error of 3.11 kcal/mol for enthalpies of formation at 298 K for the G2 test set (including radicals, nonhydrogen systems, hydrocarbons, substituted hydrocarbons, and inorganic hydrides).[36,37] In addition, the B3LYP functional has been widely used to investigate the potential energy surfaces (PES) of various systems containing H/C/O.[38−44] This functional also provides a good description of the PES of transition metal-containing molecules.[45−55] It is important to have a consistent QM method for building a training set, so we have chosen to use the B3LYP functional to build and expand the force field to describe systems such as hydrocarbons, metals, and metal oxides.

The two most popular methods of calculating charges from QM are Mulliken populations and electrostatic fitting (ESP) to the potential outside the molecule. Neither is perfect but we

find that for larger molecules small changes in the conformation can result in large changes in the ESP charges. This does not happen for Mulliken charges. On the other hand, Mulliken charges do not fit the dipole and higher moments as well as ESP. But we find that Mulliken charges do well in describing the local electronegativity and provide a self-consistent scheme for obtaining charges. Mulliken is well-suited to being used for fitting electronegativity and hardness parameters in the EEM and QEq schemes. While Mulliken charges may not precisely reproduce dipole moments and other high moments, they do well in describing the local electronegativity and are well-suited to being used for fitting electronegativity and hardness parameters in the EEM scheme[56] used in ReaxFF. Mulliken charges are well-behaved for similar systems and provide a self-consistent scheme for obtaining charges for the ReaxFF training set. In order to fit the charge parameters in the ReaxFF force field, we have calculated Mulliken charge distributions using the 6-31G** basis set.[57]

2.3. Molecular Dynamics Simulations. To simulate high-temperature gas-phase oxidation of hydrocarbons, a periodic system containing 1 hydrocarbon molecule and 100 oxygen molecules was created. The hydrocarbons studied in this investigation included methane, propene, *o*-xylene, and benzene. The use of a single hydrocarbon molecule allowed for detailed evaluation of the chemical events associated with the oxidation process. The configuration of the system containing *o*-xylene is shown in Figure 1a. The MD simulations are performed with a constant number of atoms in a constant volume where we control the temperature using a thermostat and we designate these conditions as NVT. The simulation procedure began with minimization of each system using low-temperature MD. Next, the system was equilibrated at 2500 K for 100 ps using a NVT−MD simulation with a MD time step of 0.1 fs. The systems studied are composed of flexible molecules with flexible bonds that exhibit translational, rotational, torsional, and vibrational motion. Generally, the time step should be 1 order of magnitude smaller than the shortest motion or approximately 0.5 to 1.0 fs. With ReaxFF, a smaller time step is required because the charges and bond orders are allowed to change at every time step. For high-temperature (2500 K) ReaxFF MD simulations, we have found that a time step of 0.1 fs allows for efficient coverage of the phase space and collisions and reactions to occur smoothly. The temperature was controlled using a Berendsen thermostat with a 0.1 ps damping constant.[58] During the equilibration simulations, the C−O and H−O bond parameters were switched off to prevent reactions from occurring during the equilibration of the system. The equilibrated systems were then used in NVT−MD simulations where the temperature was set to 2500 K using a temperature damping constant of 0.5 ps and a MD time step of 0.1 fs. The total simulation time for each system was determined by the extent of oxidation of the hydrocarbon and simulations were terminated when no further oxidation was observed.

To determine the initiation time required for oxidation of each hydrocarbon to start, a series of 40 NVT−MD simulations were performed at 2500 K using a temperature damping constant of 0.5 ps and a MD time step of 0.1 fs. Each of the 40 simulations had a unique starting configuration. We define initiation time as the time required for observation of the first reaction in the simulation that coincides with the disappearance of the original hydrocarbon. A second set of simulations was performed with the same MD parameters where the temperature was lowered to 2250 K to evaluate the temperature dependence of the initiation times.
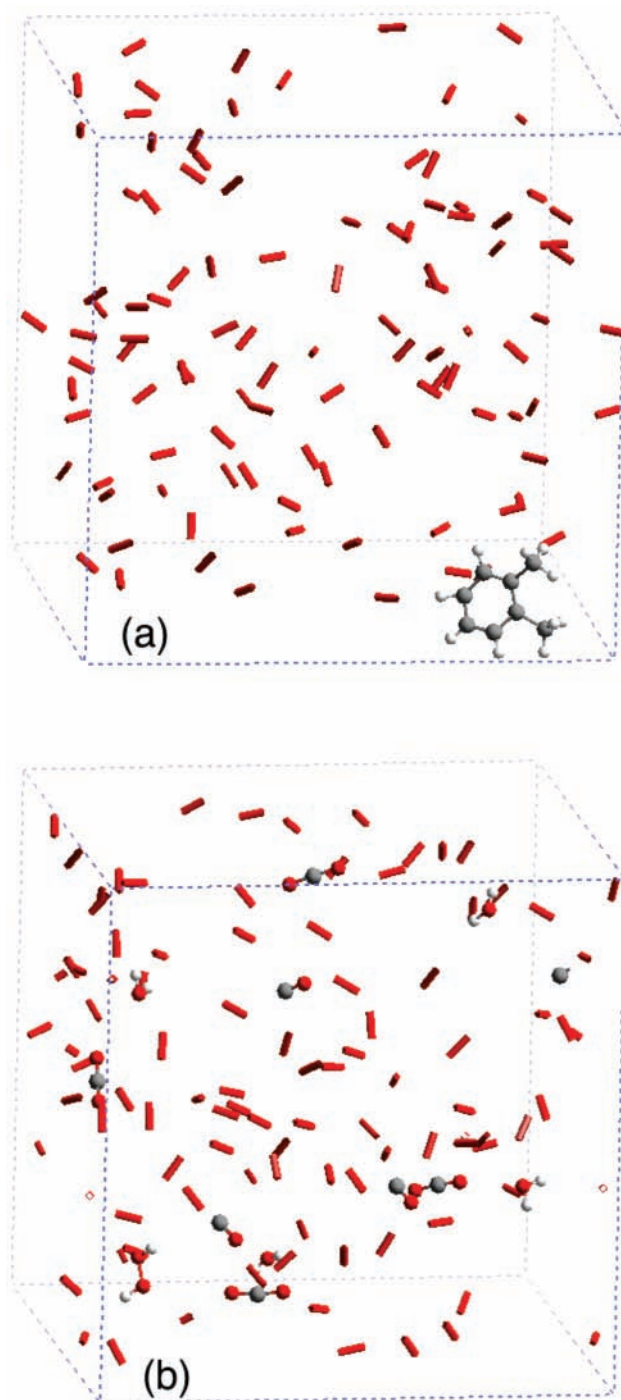

Figure 1. (a) Snapshot of the equilibrated *o*-xylene/O$_2$ system. (b) Final configuration after an 1800 ps NVT−MD simulation was performed at 2500 K. Molecular oxygen is represented by sticks and the *o*-xylene and oxidation products are represented using the ball-and-stick model.

In addition to studying the oxidation processes of individual hydrocarbons, a simulation of a mixture of hydrocarbons in an oxygen environment was performed to analyze the trend in reactivity for a complex system. The periodic system was composed of 5 molecules each of methane, propene, *o*-xylene, and benzene plus 200 molecules of oxygen. The system was minimized using low-temperature MD and then equilibrated at 2500 K using a temperature damping constant of 0.1 ps and a MD time step of 0.1 fs. Starting with the equilibrated configuration, an NVT−MD simulation was performed at 2500 K

MD Simulations of Hydrocarbon Oxidation

J. Phys. Chem. A, Vol. 112, No. 5, 2008 **1043**

TABLE 1: Equivalence Ratio, Density, and Pressure of the Systems Studied

	ϕ^a	density (g/cm^3)	pressure (GPa) equilibrated system	final configuration
methane	0.02	0.342	0.34	0.36
propene	0.045	0.345	0.36	0.35
benzene	0.075	0.348	0.36	0.36
o-xylene	0.095	0.351	0.35	0.35
hydrocarbon mixture	2.35	0.345	0.29	0.35

^{a} ϕ is the equivalence ratio.

using a temperature damping constant of 0.5 ps and a MD time step of 0.1 fs with a total simulation time of 500 ps.

Analysis of the intermediates and products formed during the simulation was performed with a 0.2 bond order cutoff for recognition of molecules. We use a low cutoff for analysis of these low-density simulations in order to capture all reactions including unsuccessful ones that produce very short-lived species. The choice of bond order cutoff does not affect the simulation itself but only the interpretation in terms of chemical components. The equivalence ratio (ϕ) and the density of the different systems studied are given in Table 1. The equivalence ratio is determined by dividing the hydrocarbon-to-oxygen ratio by the ratio required for complete combustion of the hydrocarbon to CO_2 and H_2O. In addition, the pressures of the equilibrated systems prior to starting the simulation as well as the final pressures of the systems are also given in Table 1. The pressure used for the simulations was approximately 300 MPa = 0.3 GPa = 3000 atm which can easily occur in many reactive processes, including rocket engines and shock induced reactions but may be a bit high for typical combustion conditions.

3. Results and Discussion

3.1. Parametrization of ReaxFF Force Field. To derive ReaxFF parameters for hydrocarbon oxidation chemistry, we started with the parameters for the ReaxFF hydrocarbon force field,[17] which were determined through optimization against an extensive training set obtained from ab initio calculations. This hydrocarbon ReaxFF force field, later extended for simulations of thermal decomposition of RDX[18,19] and TATP,[20] included the following data: bond dissociations for single, double, and triple bonds; angle bending energies for small molecules; charge distributions; heats of formation; relative stabilities of a wide range of small molecules; energies for molecules with under- and over-coordinated atoms; equations of state and cohesive energies for molecular crystals (since QM-methods are in general not reliable for weak van der Waals attractions, we used experimental values for the cohesive energies); and reaction mechanisms such as Diels−Alder reactions and hydrogen and methyl transfer.

In order to have a comprehensive hydrocarbon force field, we include both low energy and high-energy processes so that we have an unbiased training set. For example, it is important for the force field to describe both the high barrier for methyl transfer and the lower barrier for hydrogen transfer so that the correct reactions occur during simulations. The hydrocarbon training set was expanded with QM data describing hydrocarbon oxidation chemistry and general data describing H/C/O compounds. Thereafter, we re-optimized the ReaxFF parameters (including the originally used hydrocarbon parameters) until the force field achieved the agreement with the QM data reported in this paper.
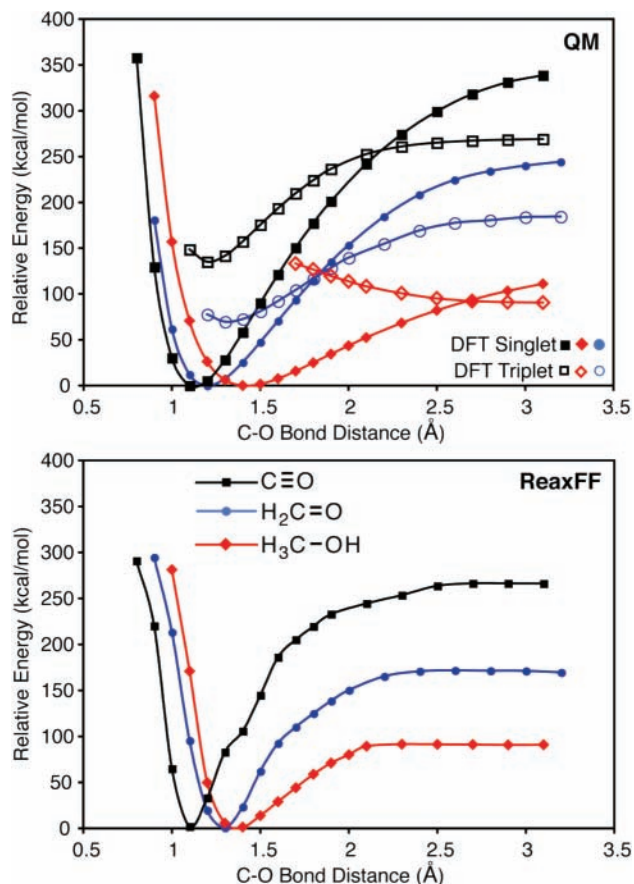

Figure 2. QM (6-311G**/B3LYP) and ReaxFF bond dissociation energies for C−O single, double, and triple bonds.

To obtain the H/C/O compound data required to extend the hydrocarbon-training set, DFT calculations were performed on the following systems: (a) dissociation energies for various bonds containing carbon, oxygen, and hydrogen. The ground-state structure was obtained through full geometry optimization. Dissociation curves were calculated by constraining only the bond length of interest and re-optimization of the remaining internal coordinates. Since the single determinant description used in DFT poorly describes the singlet state at large separation distances, we calculate the triplet state to obtain the correct dissociation energy. Therefore, multiple spin states are calculated for each dissociation curve. Since ReaxFF does not include the concept of multiple spin states, it is parametrized to reproduce the energy corresponding to the lowest energy spin state. The C−O dissociation profiles were obtained for the single bond in methanol, the double bond in formaldehyde, and the triple bond in carbon monoxide. The trend in ReaxFF C−O dissociation energy as well as the C−O bond length is in good agreement with the QM data and is shown in Figure 2. In addition, ReaxFF also provides a good representation of the dissociation energies and equilibrium bond distance for the O−O single bond obtained for HO−OH and the O−O double bond in molecular oxygen (Figure 3).

(b) To optimize the valence angle parameters for ReaxFF, DFT calculations were performed on small molecules to obtain angle distortion energies. For these calculations, angle restraints were applied to the internal coordinate of interest, and the rest of the structure was relaxed during the minimization. We included 14 molecules in the training set to cover all possible H/C/O valence angle combinations and included separate cases for angles containing single and double bonds. Figure 4 shows a comparison between ReaxFF and QM for two different valence
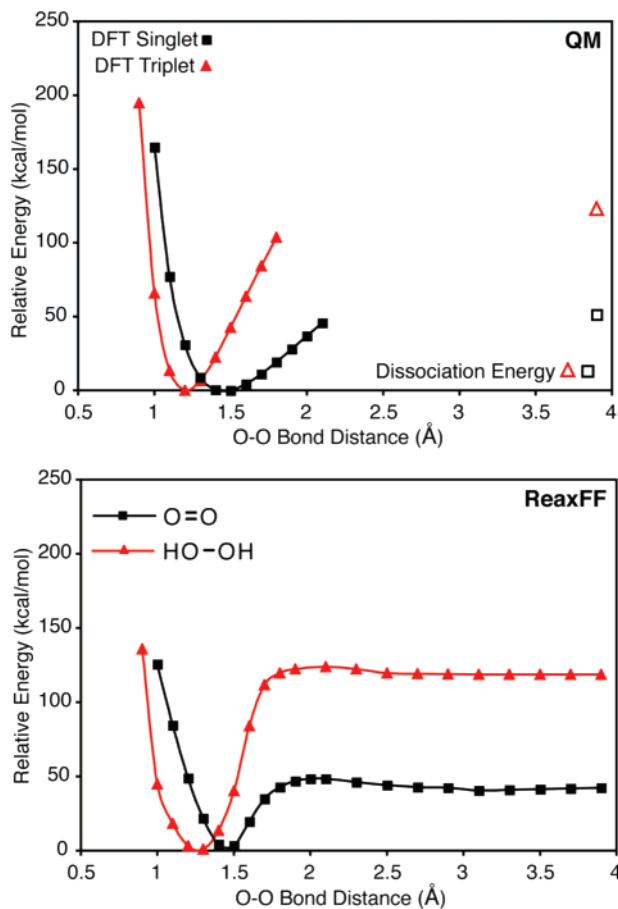
Figure 3. QM(6-311G**/B3LYP) and ReaxFF bond dissociation energies for O−O single and double bonds.

Figure 4. QM(6-311G**/B3LYP) and ReaxFF energies for distortion of C−C−O angle in ethanol (H₃C−CH₂−OH) and C−C=O in acetaldehyde (H₃C−CH₂=O).

angles: the C−C−O valence angle in ethanol and the C−C=O valence angle in acetaldehyde. In total, there are 11 different valence angle cases for structures containing C, H, and O that have been included in the training set. Comparisons between ReaxFF and QM for additional angle bending energies have been determined and these results are supplied in Supporting Information.

(c) The dihedral force field parameters were optimized against QM data describing C−C, C−O, and O−O rotational barriers in a set of 39 small molecules, describing all possible X−C−C−X, X−C−O−X, and X−O−O−X systems. Separate molecules were included for rotational barriers around single and double bonds and for single and double bonds next to the central bond. Rotational barriers were obtained by constraining the appropriate dihedral angle and subsequent relaxation of the molecule. Figure 5 shows a comparison between QM and ReaxFF for four of these rotational barrier cases. The dihedral angle, C−C=C−O, in 1-propen-1-ol has the largest rotational barrier compared with the three other cases, which involve rotation around single bonds. ReaxFF is able to reproduce this feature well. The results for the remaining 35 rotational barriers that were included in the training set for parametrization of ReaxFF are supplied in Supporting Information.

(d) The EEM charge parameters[56] used in ReaxFF (electronegativity, hardness and shielding for each element) were optimized against Mulliken charge distributions obtained from DFT calculations. There are other alternatives for optimizing charge parameters. Thus, Bourasseau et al.[59] use dipole and partial charges from a QM condensed phase system. Figure 6 shows a comparison between the Mulliken charge distributions from QM and the charge distributions obtained from ReaxFF
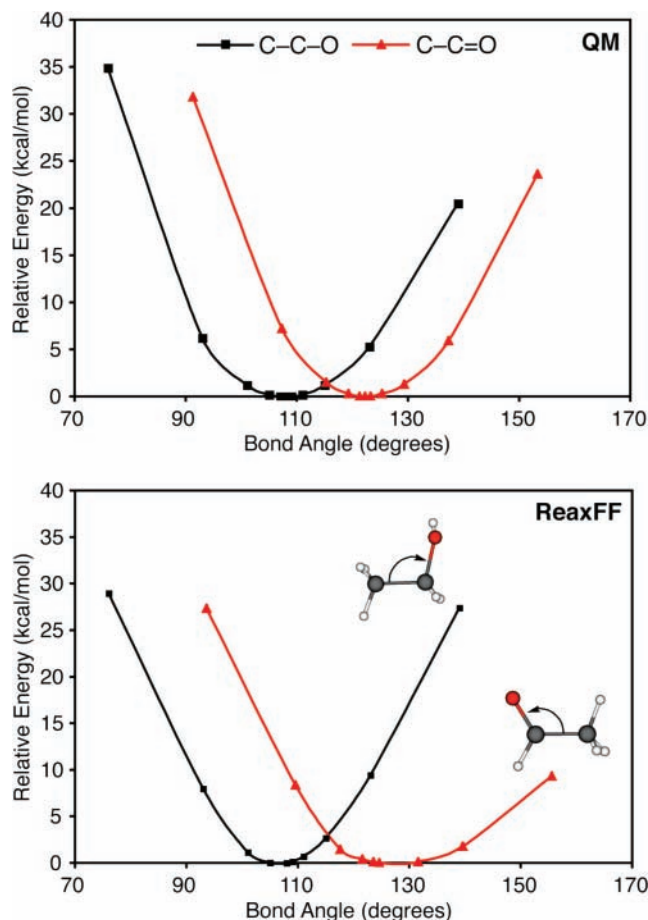
for formic acid and hydroperoxy-methanol. ReaxFF successfully reproduces the charge assignments for these structures.

(e) We added a number of reaction energies and mechanisms relevant to hydrocarbon oxidation to the hydrocarbon training set. Since the reaction of O₂ with a hydrocarbon molecule is vital to combustion chemistry, DFT calculations were performed to determine the reaction profile for molecular oxygen abstracting a hydrogen from a methanol molecule as a function of R_{C−O}, the distance between the carbon atom in the methanol and an oxygen atom in O₂. Methanol was used as a model system because of the difference in C−H versus O−H bond strength. The results for abstraction of the methyl C−H hydrogen are shown in Figure 7a, and the results for abstraction of the hydroxyl O−H hydrogen are shown in Figure 7b. ReaxFF correctly describes the height of the barrier for hydrogen abstraction for the two types of hydrogens. As the C−O distance is increased from 2.5 to 3.5 Å, the barrier for hydrogen abstraction increases for both cases and ReaxFF is able to reproduce this feature. Also included in the training set is the reaction mechanism for three Diels−Alder reactions. These included the 4 + 2 cycloaddition of O₂ with butadiene, benzene, and cyclopentadiene (Cp). DFT calculations are performed by symmetrically constraining both C−O bond lengths at each distance of interest while relaxing the other geometrical parameters during the minimization, and the results are shown in Figure 8. The Diels−Alder reaction profiles calculated using ReaxFF (Figure 8) provide an accurate description of the stabilities of the reactants and products, the size of the barrier, and the energetic differences between the three different reactions. In addition to the H abstraction and Diels−Alder
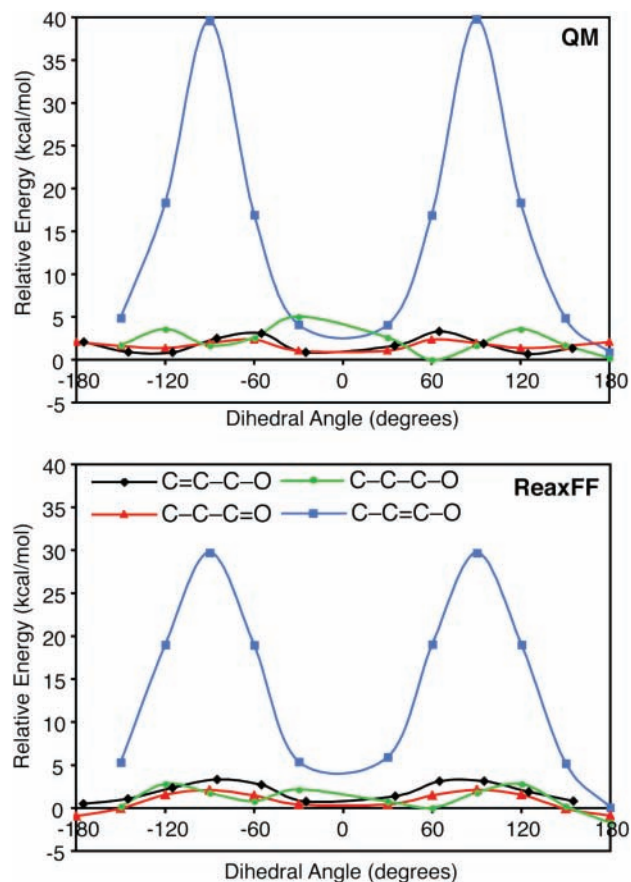
MD Simulations of Hydrocarbon Oxidation

J. Phys. Chem. A, Vol. 112, No. 5, 2008 **1045**

Figure 5. QM(6-311G**/B3LYP) and ReaxFF rotational barriers for the following dihedral angles: C—C—C—O in propanol (H$_3$C—CH$_2$—CH$_2$—OH), C=C—C—O in 2-propen-1-ol (H$_2$C=CH—CH$_2$—OH), C—C=C—O in 1-propen-1-ol (H$_3$C—CH=CH—OH), and C—C—C=O in propanal (H$_3$C—CH$_2$—CH=O).
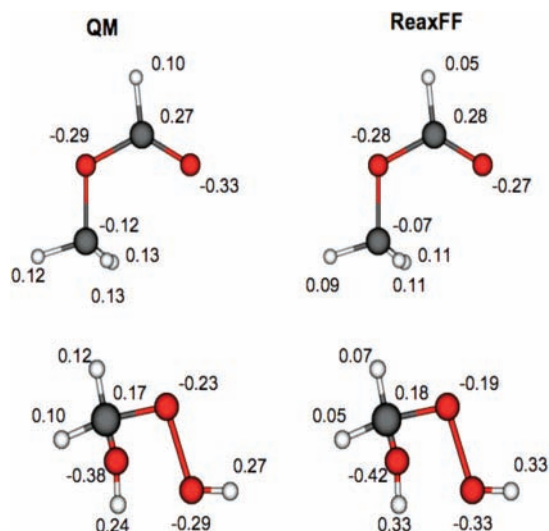
Figure 6. Comparison of Mulliken charge distributions obtained from QM(6-31G**/B3LYP) and charge distributions obtained from ReaxFF.

reactions, comparisons between ReaxFF and QM for other reactions relevant to hydrocarbon oxidation are supplied in Supporting Information. The ability of ReaxFF force field to successfully describe the diverse training set provides a useful tool to investigate the pre-ignition chemistry of combustion.

3.2. Molecular Dynamics Simulations of Hydrocarbon Oxidation. *3.2.1. Oxidation of a Single Hydrocarbon Molecule.* An NVT—MD simulation of the high-temperature (2500 K)

oxidation of the simplest hydrocarbon, methane, exposed to oxygen molecules was used as a first test for the ReaxFF force field. Figure 9 shows the time evolution of the intermediates and products observed during the simulation. The change in the potential energy (Figure 9) during the simulation illustrates the exothermicity of the oxidation process. A detailed analysis of each step leading to the oxidation of methane is shown in Scheme 1, where the boxes indicate formation of the final products. The oxidation of methane is initiated by hydrogen abstraction by molecular oxygen to form hydroperoxyl and methyl radical species. Radical—radical combination of these two species leads to methyl hydroperoxide. By using a low-temperature (25 K) constrained MD simulation to drive the reaction coordinate, the initial reaction observed for methane (CH$_4$ + O$_2$ → CH$_3$ + HO$_2$) is endothermic with a barrier of ∼50 kcal/mol. The barrier for the reverse reaction (CH$_3$ + HO$_2$ → CH$_4$ + O$_2$) is very small (∼8 kcal/mol) indicating that if the radicals would remain nearby each other, the reverse reaction might occur. The second reaction, CH$_3$ + HO$_2$ → CH$_3$—OOH, is barrierless and exothermic. Therefore, it is more likely that CH$_3$ + HO$_2$ will result in CH$_3$—OOH rather than CH$_4$ + O$_2$ as observed in the ReaxFF MD simulation. In this simulation, the CH$_3$—OOH molecule exists for only 0.72 ps until the weak O—O bond breaks to form the hydroxyl and methoxy radical species. The methoxy radical is unstable and decomposes to formaldehyde and a hydrogen radical, which is consistent with rate measurements and identification of the products in experiments.[1,2]

The hydrogen radical quickly reacts with molecular oxygen to form a new hydroperoxyl radical. Of course, the H radical could have recombined with the hydroxyl radical produced in the previous step. Although we have observed such recombinations in other systems, we saw no such events in this simulation, probably because of the low concentration of H and OH radicals compared with the relatively large concentration of O$_2$. Next, the hydroxyl radical attacks the formaldehyde and through a hydrogen abstraction reaction forms water and formyl radical. Previous experimental[60-62] and theoretical[62,63] investigations of this reaction agree that a hydrogen from the formaldehyde is abstracted by the hydroxyl radical and that addition of the hydroxyl radical to the formaldehyde would proceed via a transition state which is higher in energy. Xu et al.[63] recently calculated the barriers at the 6-311+G(3df,2p)/CCSD level of theory for the H abstraction to be 2.6 kcal/mol and calculated that for the OH addition to be 5.7 kcal/mol. This can be compared to barriers obtained using low-temperature constrained MD in ReaxFF to drive the reaction coordinates. We find the hydrogen abstraction barrier to be ∼7 kcal/mol and the barrier for OH addition to be ∼4 kcal/mol. Since these specific reaction pathways were not included in the training set, this suggests that ReaxFF predicts low barriers for both processes to within ∼5 kcal/mol.

The reaction pathway proceeds by radical combination of the hydroperoxyl and formyl radicals resulting in performic acid [HCO(OOH)] formation. Homolytic bond cleavage of the O—O bond forms the hydroxyl and formate radical species and this is followed by intramolecular rearrangement of the formate radical to H—O—C—O and then dissociation of another hydroxyl radical to produce carbon monoxide. At the high temperature and pressure conditions of the simulation, intramolecular rearrangements of formate radical are energetically accessible.

Note that we do see the H—O—C=O radical species, which eventually decomposes into HO + CO, rather than H + CO$_2$. This is because H—O—C=O is 11.4 kcal/mol more stable than
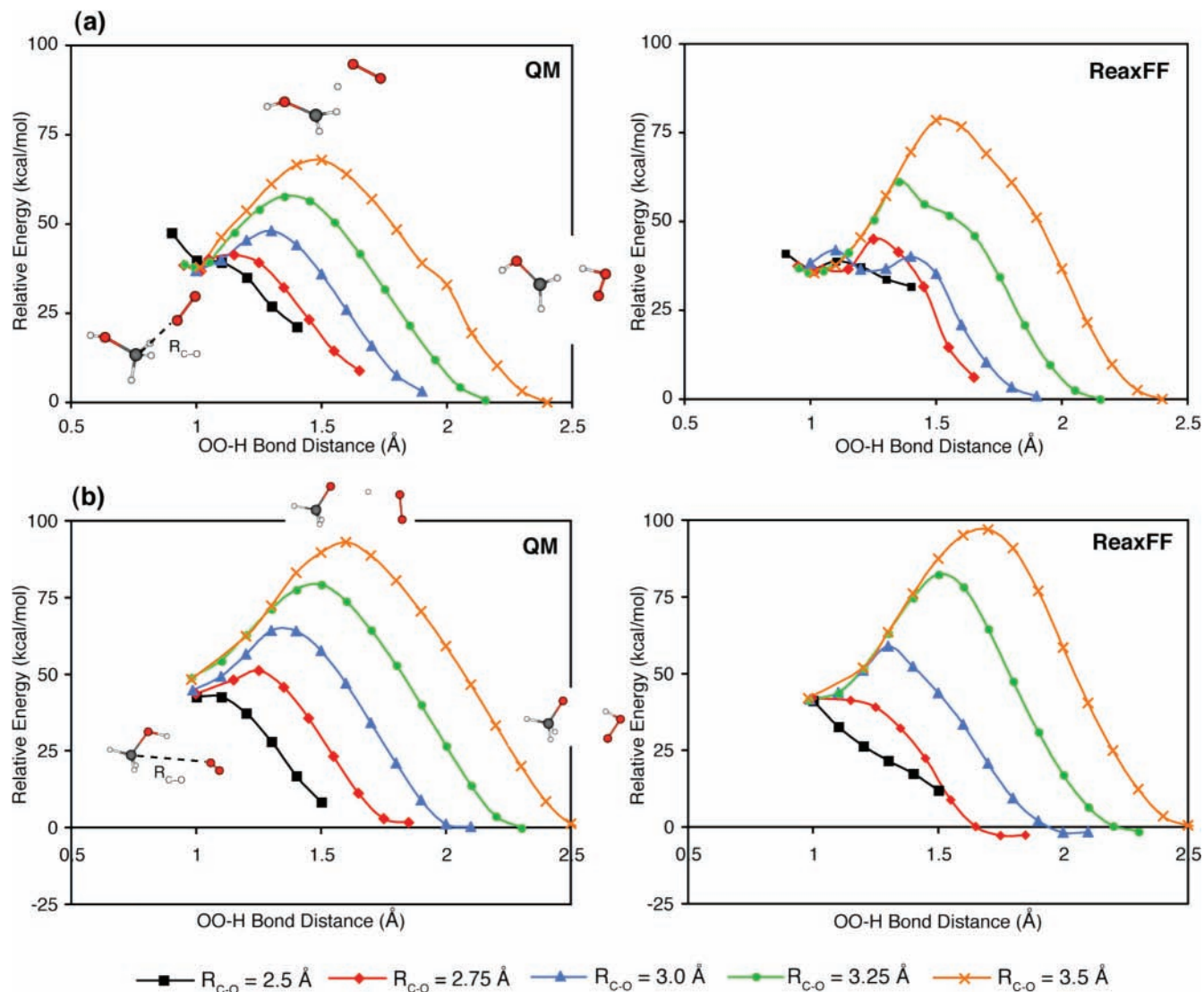
Figure 7. QM(6-311G**/B3LYP) and ReaxFF potential energy surface for (a) the formation of hydroperoxyl radical by methyl hydrogen abstraction from methanol by molecular oxygen and (b) the formation of hydroperoxyl radical by hydrogen abstraction from the alcohol group of methanol by molecular oxygen. The reaction profile is also shown for a range of $C-O_2$ distances (R_{C-O}).

the formate radical and 6.56 kcal/mol more stable than H + CO_2 (calculated using 6-311G**/B3LYP).

The final products observed from the NVT−MD simulation include carbon monoxide, water, and two hydroxyl radicals. The simulation was continued for an additional 1500 ps to determine if the final product distribution would continue to change. The extended simulation time did not result in further oxidation of CO to CO_2; this is consistent with this process being relatively slow and occurring later in combustion reactions once the fuel is essentially consumed.[9]

The intermediates observed during the oxidation of methane, $CH_3 \rightarrow CH_2O \rightarrow CHO \rightarrow CO$, are consistent with results obtained from kinetic modeling studies.[1,2,64−66] At longer time scales, it is expected that the remaining hydroxyl radicals in the simulation would react with the carbon monoxide to complete the combustion of methane to carbon dioxide.

Although there are 100 molecules of O_2 available during the simulation, only 2 molecules directly participate in the oxidation of methane. Analysis of the trajectory show numerous collisions of O_2 with various intermediates, but most of these collisions do not lead to reactions, allowing time for other radicals in the system to participate in the oxidation process.

Proceeding to more complicated hydrocarbons, a 2500 K NVT−MD simulation was performed on a system containing 100 oxygen molecules and 1 propene molecule. Propene is an important intermediate olefin and forms in the early stages of combustion of propane and higher alkanes. Because of the high reactivity of alkenes, the detailed study of their oxidation mechanism is more challenging than simple alkanes for experimentalists. However, ReaxFF simulations allow for the study of the reaction mechanism for any molecule including unsaturated hydrocarbons and radical intermediates. Figure 10 shows the time evolution of the various intermediates and products observed during the NVT−MD simulation of propene oxidation. The oxidation of propene is highly exothermic as shown by the change in potential energy (Figure 10). The initiation step involves hydrogen abstraction of the methyl hydrogen from propene by molecular oxygen to form the resonance stabilized allyl radical and a hydroperoxyl radical at 195 ps. The allylic C−H bond is relatively weak compared with the methylene C−H bond, making it the energetically favored abstraction reaction for propene. Kinetic models based on experimental results indicate that hydrogen abstraction reactions are important in the propene consumption pathway[67−68] par-
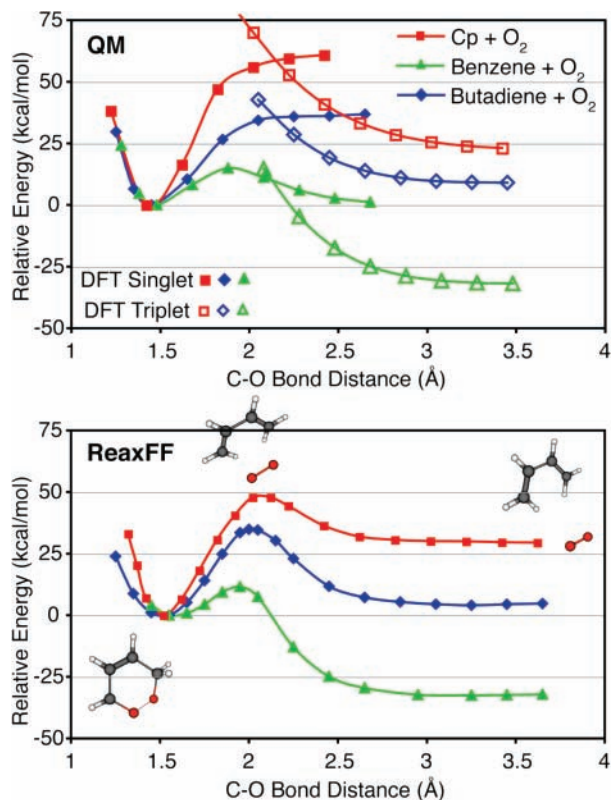
MD Simulations of Hydrocarbon Oxidation

J. Phys. Chem. A, Vol. 112, No. 5, 2008 **1047**

Figure 8. QM(6-311G**/B3LYP) and ReaxFF reaction profile for the 4 + 2 cycloaddition of O_2 with butadiene, benzene, or cyclopentadiene (Cp).
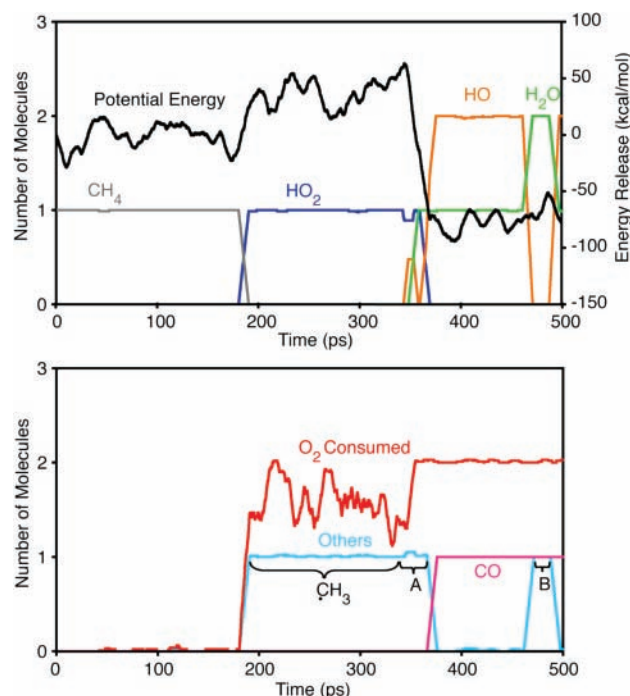

Figure 9. Product distribution observed in the NVT−MD simulation of methane in an O_2 atmosphere. Only major products are shown explicitly; all intermediates and minor products are included as "others" which is divided into three segments showing presence of methyl radical, the short-lived intermediates from oxidation of methyl radical (A), and the recombination of hydroxyl radicals to form hydrogen peroxide (B).

ticularly at fuel lean conditions[69] and above 1700 K.[70] Internal hydrogen transfer in the allyl radical yields $H_3C-C≡CH_2$ radical which undergoes hydrogen abstraction by molecular
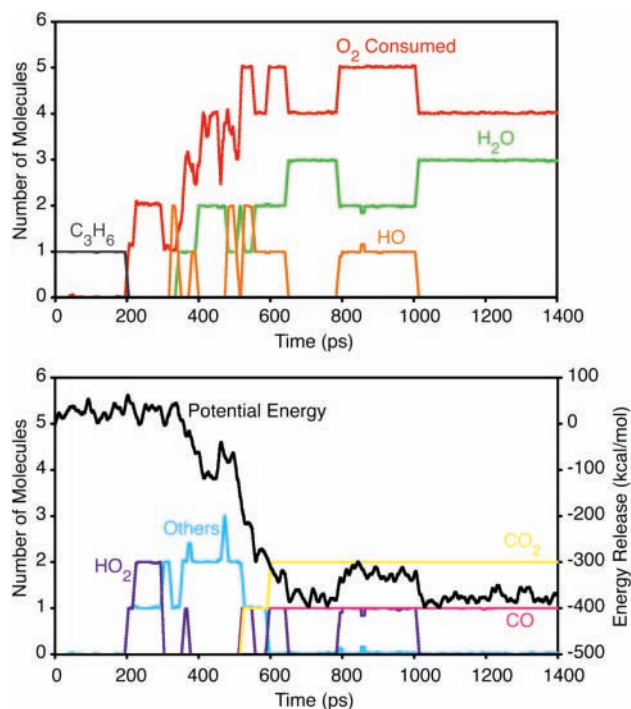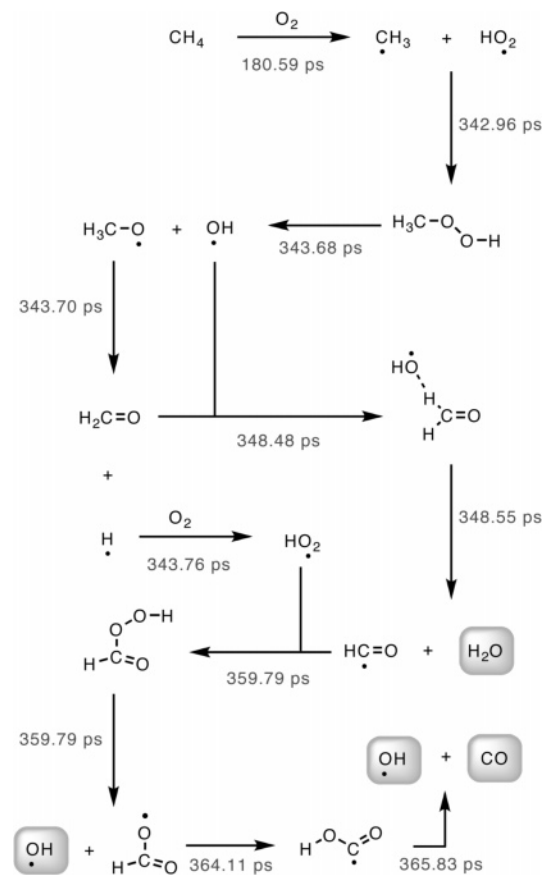

Figure 10. Product distribution observed in the NVT−MD simulation of propene in an O_2 atmosphere. Only major products are shown explicitly; all intermediates and minor products are included as "others".

SCHEME 1: Methane Oxidation Pathway Observed during ReaxFF NVT−MD Simulation

oxygen to form an additional hydroperoxyl radical and allene. The presence of allene has been observed in trace quantities during a jet stirred reactor experiment performed by Dagaut et al.[71] A detailed reaction scheme is included in Supporting

Information and shows the initial steps of the oxidation already discussed as well as the steps showing the further oxidation of allene leading to production of three water molecules, a carbon monoxide molecule, and two carbon dioxide molecules.

During this simulation, the carbon dioxide was not formed from conversion of carbon monoxide but directly from oxygen-containing carbon radical species. It has been suggested that any carbon dioxide formed during combustion is converted from carbon monoxide primarily by reaction with hydroxyl radicals or secondarily by recombination with oxygen.[2] Detailed analysis of the reaction pathways for oxidation of propene at 2500 K suggests that carbon dioxide can also be formed directly under fuel lean conditions. In the ReaxFF MD simulation, one CO_2 is produced via hydrogen dissociation from H−O−C−O radical. The second CO_2 formed in the oxidation of propene involves O_2 attack on an HCO radical resulting in the production of CO_2 and a hydroxyl radical. Then, hydroxyl radical combines with a hydrogen radical in the system to form water. Since no hydroxyl or hydroperoxyl radicals are present at the end of the NVT−MD simulation, conversion of carbon monoxide to carbon dioxide could only take place through recombination with oxygen.

o-Xylene is the most complex hydrocarbon whose oxidation was studied. The *o*-xylene molecule was equilibrated in a periodic box with 100 oxygen molecules and the configuration of the equilibrated system is shown in Figure 1a. Next, an NVT−MD simulation was performed at 2500 K for 1800 ps, and the final configuration from this simulation is shown in Figure 1b. The time evolution of the intermediates and products observed during the simulation are presented in Figure 11. As shown by the change in potential energy (Figure 11), the oxidation of *o*-xylene is the most exothermic of the hydrocarbons studied. Scheme 2 provides a detailed analysis of reactions leading to oxidation of the aromatic ring and formation of hydrocarbon chain where the boxes indicate the formation of products observed at 1048 ps. The initial reactive event is similar to methane and propene oxidation where the methyl hydrogen is abstracted by molecular oxygen resulting in the formation of the xylyl and hydroperoxyl radical species. This is consistent with experiments that suggest that ring reactions are secondary to reactions involving the side chains.[72]

Next, radical−radical combination occurs to form *o*-methylbenzyl hydroperoxide where the high-energy O−O bond is cleaved to form hydroxyl and *o*-methyl benzyl alcohol radical species. The *o*-methyl benzyl alcohol radical undergoes homolytic C−C bond cleavage to form formaldehyde and *o*-tolyl radical. Indeed these results are consistent with QM calculations (6-311G**/B3LYP), which find the reaction energy for formation of formaldehyde and *o*-tolyl radical from *o*-methyl benzyl alcohol radical to be 4.14 kcal/mol. In comparison, an alternative pathway that would produce *o*-toluadehyde and a hydrogen radical could proceed via dissociation of a hydrogen from *o*-methyl benzyl alcohol to form *o*-tolualdehyde requiring 21.9 kcal/mol. This indicates that formation of formaldehyde and *o*-tolyl radical is energetically favorable, which is consistent with the reaction observed in the simulation. Molecular oxygen binds to the *o*-tolyl radical forming 2-methylphenyldioxy radical, which undergoes intermolecular hydrogen abstraction and dissociation of hydroxyl radical to form 6-methylene-2,4-cyclohexadien-1-one with loss of aromaticity. After 55 ps of simulation time, the ring in 6-methylene-2,4-cyclohexadien-1-one opens to form the 1,3,5,6-heptatetraen-1-one. The 1,3,5,6-heptatetraen-1-one is further oxidized to form four molecules each of water, carbon monoxide, and carbon dioxide as well as
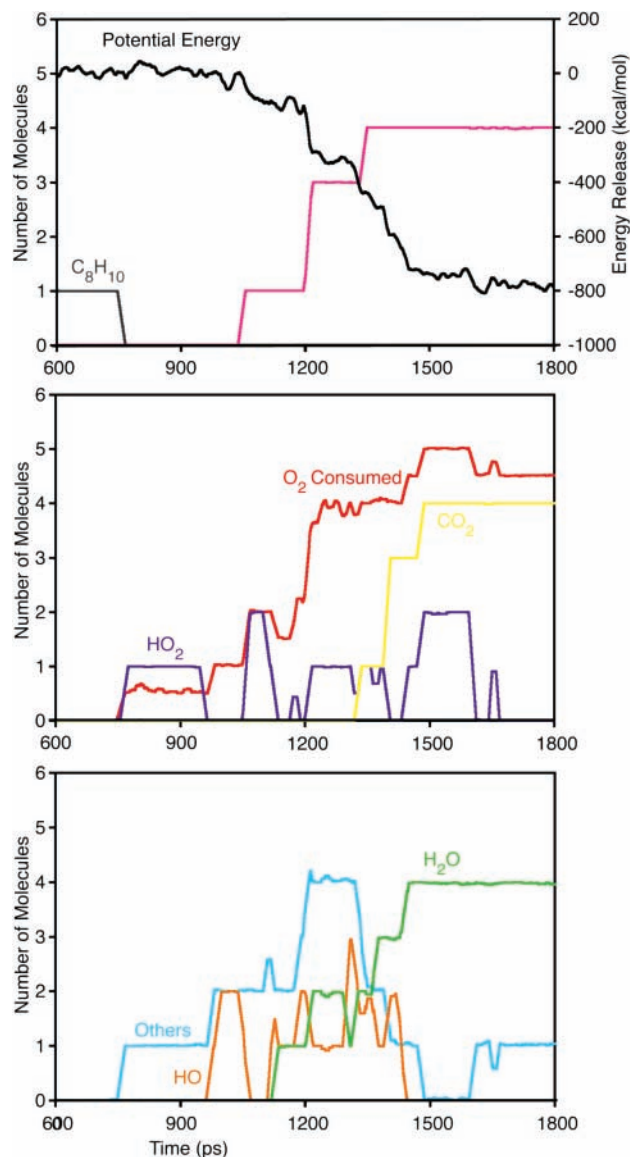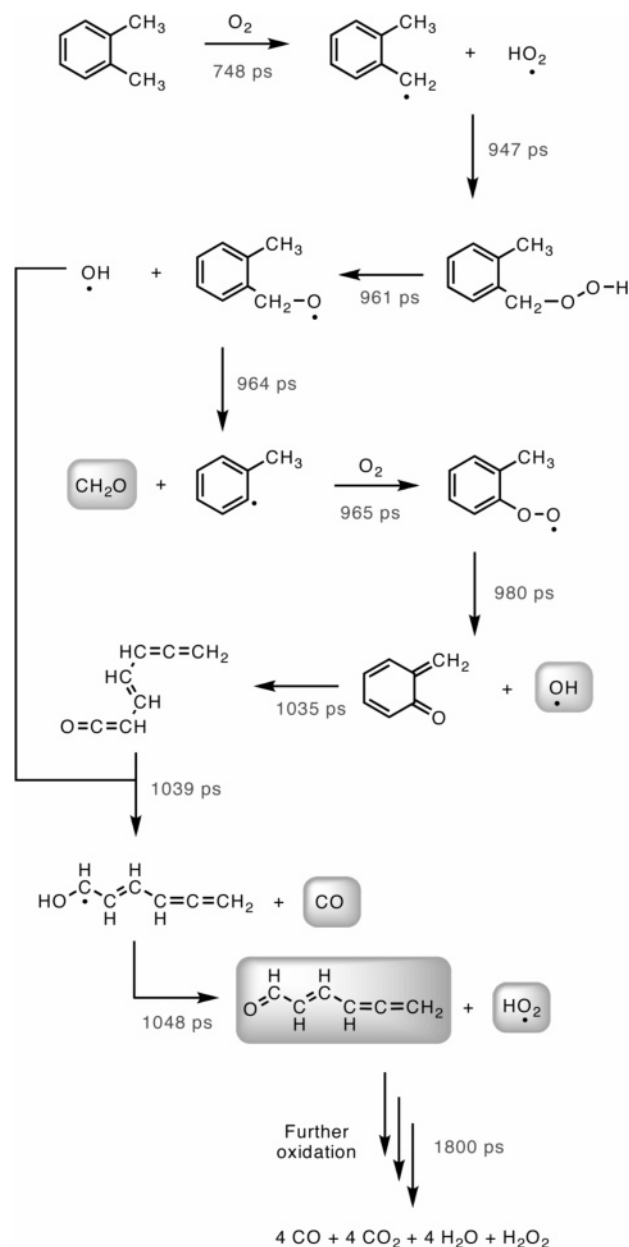

Figure 11. Product distribution observed in the NVT−MD simulation of *o*-xylene in an O_2 atmosphere. The number of oxygen molecules consumed has been divided by 2. Only major products are shown explicitly; all intermediates and minor products are included as "others".

a molecule of hydrogen peroxide after 1800 ps of simulation. The hydrogen peroxide is converted to two hydroxyl radicals during the simulation at 2500 K.

3.2.2. Reactivity of Hydrocarbons. A series of 40 unique NVT−MD simulations were performed for each of the hydrocarbons studied including benzene, methane, propene, and *o*-xylene. These simulations consisted of one hydrocarbon molecule and 100 molecular oxygens at 2250 K and 2500 K. The time required for initiation as well as the reactive event associated with the initiation were determined for each simulation. The initiation times determined for each of the 40 simulations are shown in Figure 12 for methane (CH_4), propene (C_3H_6), and *o*-xylene (C_8H_{10}). At 2250 K, methane has longer initiation times and is less reactive than both propene and *o*-xylene, which have similar initiation times. The initiation times observed at 2500 K are about the same for the molecules studied. There is a large spread in the initiation times, but we could use this method to obtain a statistically meaningful average initiation time by performing significantly more simulations. The least reactive of the hydrocarbon molecules studied was benzene, and it was unreactive in all of the NVT−MD simulations which

MD Simulations of Hydrocarbon Oxidation

J. Phys. Chem. A, Vol. 112, No. 5, 2008 **1049**

SCHEME 2: *o*-Xylene Partial Oxidation Pathway Observed in the ReaxFF NVT−MD Simulation

Figure 12. Initiation times obtained for methane (CH_4), propene (C_3H_6), and *o*-xylene (C_8H_{10}) at 2250 K and 2500 K. Initiation time is the time required for observation of the first reaction in the simulation that coincides with the disappearance of the original hydrocarbon.

were terminated at 2700 ps. This is consistent with the C−H bond in benzene being the strongest compared with the methyl C−H bonds in methane, propene, and *o*-xylene where the experimental bond dissociation energies for benzene, methane, and propene are 112.9, 104.9, and 88.8 kcal/mol, respectively.[73] In addition, C−H bond dissociation energy for the methyl H in *o*-xylene is expected to be comparable with the methyl C−H bond in toluene, which is 89.9 kcal/mol.[73] Methane has the next strongest methyl C−H bond and has the longest initiation time when compared to propene and *o*-xylene. Activation of methane at 2500 K occurs through hydrogen abstraction by molecular oxygen in all of the simulations. However, at 2250 K, 5% of the simulations were initiated by O_2 insertion into the C−H bond followed by homolytic bond cleavage to form hydroxyl and methoxy radical species.

Propene and *o*-xylene have similar initiation times with propene being slightly slower to react and this is consistent with the strength of the methyl C−H bonds. The predominant reaction pathway for initiation involves molecular oxygen
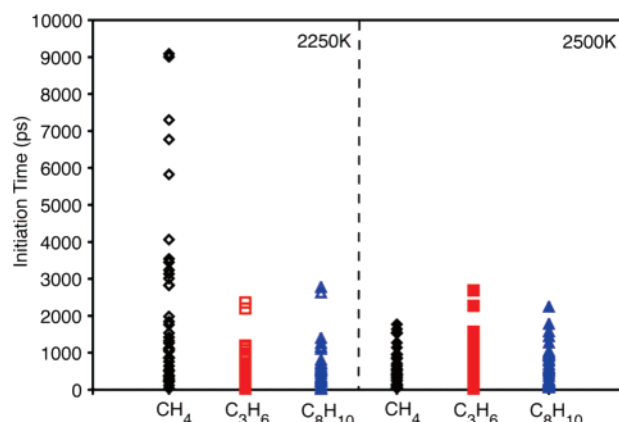
abstraction of a methyl hydrogen forming the hydrocarbon radical and the hydroperoxyl radical. Alternatively, 10% of the propene oxidation simulations at 2500 K were initiated by addition of molecular oxygen to form acetaldehyde and formaldehyde. This is consistent with experimental studies that have observed the production of acetaldehyde during the oxidation of propene.[68,71] Another minor initiation reaction observed involved formation of the formylmethyl and methoxy radical species with addition of O_2 in one simulation. At 2250 K, there were three different initiation events observed in 10% of the propene oxidation simulations. These involved (1) homolytic bond cleavage to form ethenyl and methyl radicals, (2) insertion of O_2 into the methyl C−H bond followed by breaking the high-energy O−O bond to form allyloxy and hydroxyl radical species, and (3) dissociation of H_2 from propene to form allene. Three alternatives to the H abstraction by molecular O_2 initial reactive event for *o*-xylene were observed in 10% of the simulations performed at 2500 K. These alternative initiation reactions included (1) insertion of O_2 into the methyl C−H bond followed by dissociation of the high-energy O−O bond to form the benzylalcohol and hydroxyl radicals, (2) O_2 into the C−CH_3 bond followed by dissociation of the high-energy O−O bond to form *o*-methylphenoxy and methoxy radical species, and (3) dissociation of H_2 from the *o*-xylene methyl groups to form *o*-xylylene (5,6-bis(methylene)-1,3-cyclohexadiene). The formation of *o*-xylylene has been experimentally observed in flow reactor experiments.[72]

The series of ReaxFF NVT−MD simulations have allowed for the observation of multiple initiation pathways for oxidation of individual gas-phase hydrocarbon molecules in a high-temperature and very lean combustion environment with an equivalence ratio of 0.02 to 0.095. The most important reactive event for initiation is the abstraction of hydrogen from the methyl group and the delay until initiation for the hydrocarbons studied is consistent with the trend in the strength of that C−H bond involved in the reaction. By analyzing the initial chemical events of each simulation, a number of secondary initiation pathways were also observed. Additional simulations could be performed to investigate the effect of more than one hydrocarbon molecule and changes in the equivalence ratio on the delay in initiation and the types of initiation pathways that are observed for the various hydrocarbons.

3.2.3. Oxidation of a Mixture of Hydrocarbon Molecules. A 2500 K NVT−MD simulation was performed with 200 molecules of O_2 and 5 molecules each of benzene, methane, propene, and *o*-xylene with a total of 620 atoms (Figure 13a).

Figure 14. Reactant distribution observed during the NVT−MD simulation of a mixture of hydrocarbons in an O_2 atmosphere. The number of oxygen molecules consumed has been divided by 4. Only major products are shown explicitly; all intermediates and minor products are included as "others".
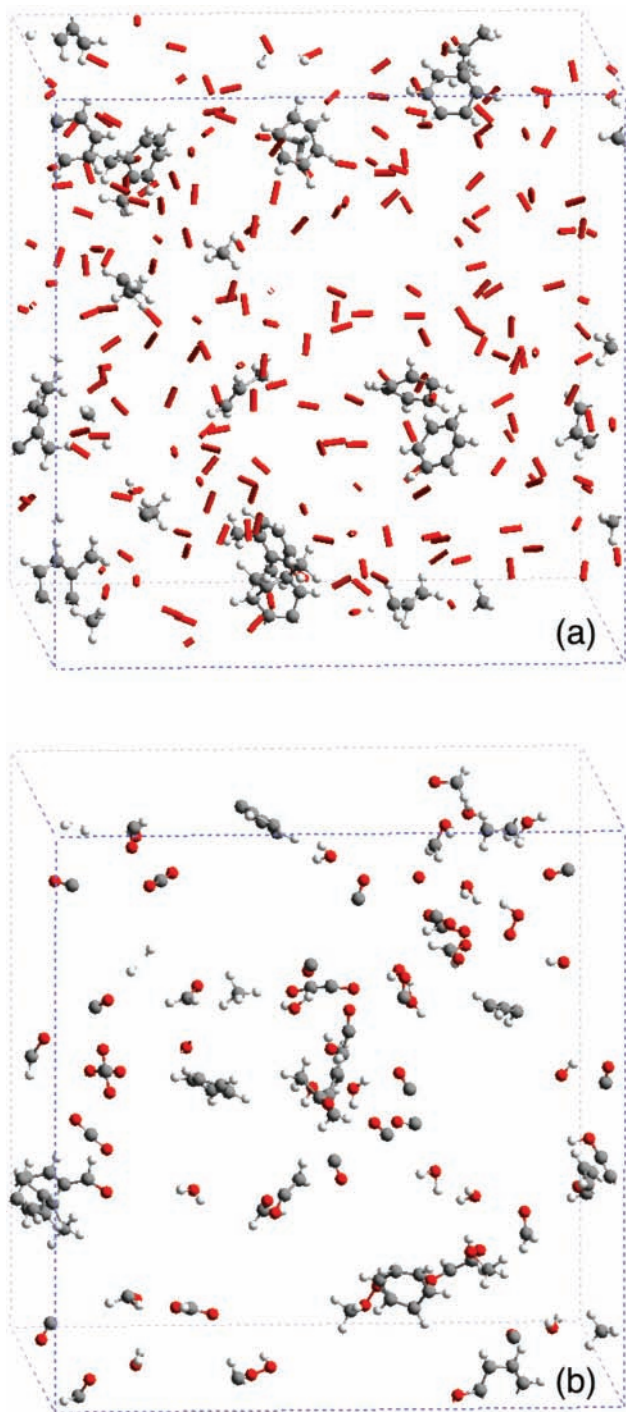
Figure 13. (a) Snapshots of equilibrated system containing a mixture of methane, propene, benzene, *o*-xylene, and oxygen. Molecular oxygen is represented by sticks and the hydrocarbons are represented by the ball-and-stick model. (b) Final configuration of system after 500 ps NVT−MD simulation. The oxygen molecules have been removed from the snapshot of the final configuration to show products formed during the simulation.

The equivalence ratio for this system is 2.35 and the combustion environment is fuel rich so there will be incomplete conversion to full combustion products. Figure 13b shows the final configuration of the oxidation products after 500 ps of simulation. The pressure of the final configuration increased by 60 MPa compared with the initial equilibrated system. The rate of consumption of the hydrocarbon reactants is shown with O_2 consumption in Figure 14. New initiation chemistry was
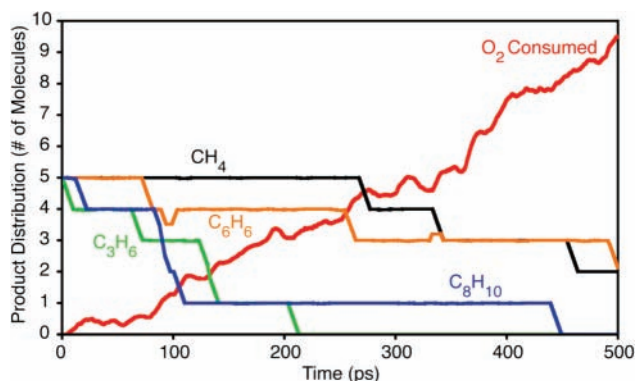
observed for the fuel rich oxidation compared to the oxidation of isolated hydrocarbon molecules at very low equivalence ratios. The first hydrocarbon to decompose was propene, which underwent homolytic bond cleavage to form the ethenyl and methyl radical species. The kinetic model study performed by Dagaut et al.[68] indicates that under fuel rich conditions the decomposition pathway may be more important than hydrogen abstraction. Hydrogen dissociation from the methyl group of *o*-xylene to form hydroperoxyl and xylyl radicals occurred next. Activation of benzene was not expected so early in the simulation because of its unreactivity in NVT−MD simulations of a single benzene molecule with O_2. In this simulation, the activation was facilitated by a methylperoxy radical, which results in formation of 2,4-cyclopentadiene-1-carboxaldehyde and a methoxy radical. Methane was the last hydrocarbon to react in the simulation with a phenoxyl radical abstracting a hydrogen to form a methyl radical and phenol. Since this system was relatively rich in hydrocarbons, the initiation reactions observed involved both decomposition and reactions with radicals in the system instead of direct oxidation of the hydrocarbons by molecular oxygen as observed in the lean fuel cases studied.

From the distribution of the products observed during the simulation shown in Figure 15, the number of intermediates and minor products, which are collectively referred to as "others", increases steadily over the coarse of the simulation and the radical species are responsible for consumption of the benzene, *o*-xylene, and methane molecules whereas the remaining propene is consumed only by hydroxyl radicals. On the basis of the chemical kinetic mechanism that Wilk et al.[67] and Thomas et al.[74] have used to model propene oxidation, hydroxyl radical addition is also an important propene consumption pathway. Minor products formed from radical−radical recombination were also observed during the simulation. A complete list of the "others" observed after 500 ps of simulation have been defined in Table 2. The high-energy O=C=C=O fragment is expected to decompose to two carbon monoxide molecules if the simulation was continued. The amount of hydroxyl and hydroperoxyl radicals in the systems does not accumulate but is consumed by reacting with hydrocarbon fragments during the simulation. Figure 15 also shows that the concentration of formaldehyde increases during the simulation, and this is consistent with production of large amounts of formaldehyde during pre-ignition and the subsequent slow decomposition of formaldehyde.[9] The amount of carbon monoxide in the system does build up over time, and at the end of the simulation, there
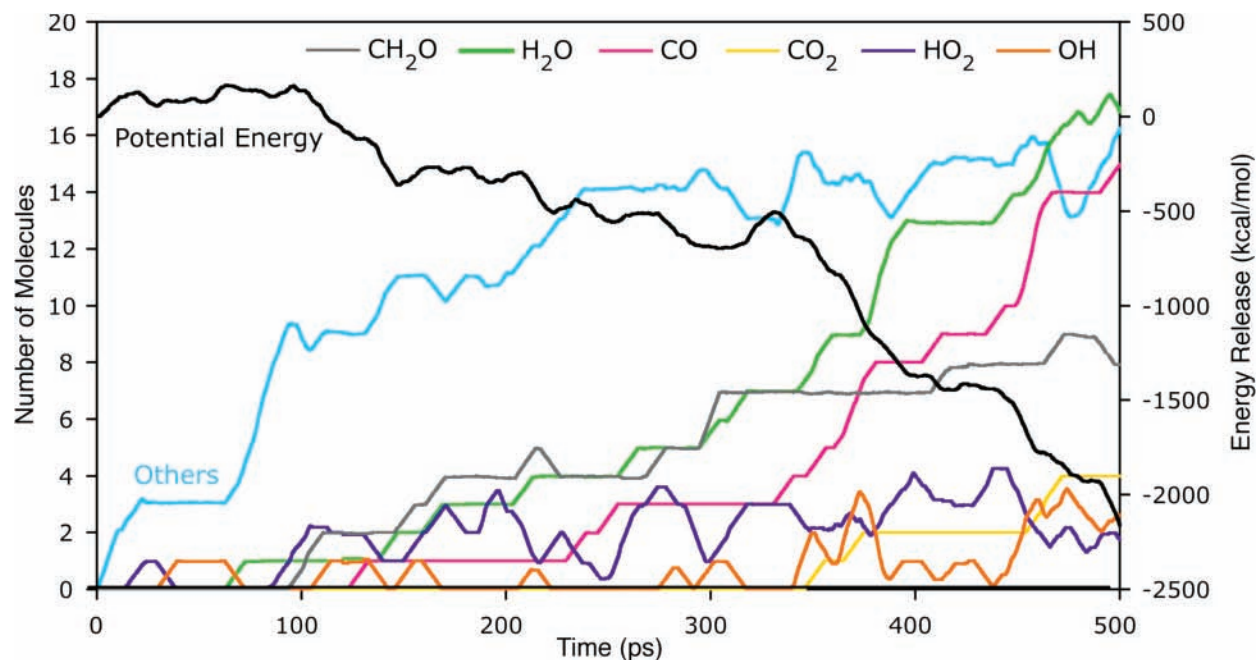
MD Simulations of Hydrocarbon Oxidation

J. Phys. Chem. A, Vol. 112, No. 5, 2008 **1051**

Figure 15. Product distribution observed at 500 ps for the NVT−MD simulation of a mixture of hydrocarbons in an O_2 atmosphere. Only major products are shown explicitly; all intermediates and minor products are included as "others".

TABLE 2: Minor Products[a] Observed in the Final Configuration from the NVT−MD Simulation of the Oxidation of a Mixture of Hydrocarbons

Number of Molecules	Structure
1	
1	
1	
1	
3	
2	HC≡C−OH
1	
1	H_3C−OH
1	O=C=C=O
1	
1	H_2
1	
1	H_2C=C=CH

[a] Minor products were grouped as "others" in Figure 14.

are 15 molecules of CO compared with 4 molecules of CO_2. Since the mixture is fuel rich, there will not be enough oxygen available for complete combustion of the hydrocarbons to carbon dioxide and water.

4. Conclusion

We have described an application of the ReaxFF reactive force field for elucidating the mechanisms for the initial steps of hydrocarbon combustion. ReaxFF was parametrized against a large and varied QM-based training set, describing bond dissociation profiles, valence and torsion angle distortion, charges, and reaction energies. To demonstrate the validity of the ReaxFF approach for simulation of combustion chemistry, we performed a range of molecular dynamics simulations on hydrocarbon/O_2 mixtures.

The dominant initiation reaction observed during simulations under fuel lean conditions is hydrogen abstraction. On the basis of the strength of the methyl C−H bond in the hydrocarbons, the delay in initiation was longest for methane compared with propene and *o*-xylene, which had comparable initiation delays. In the simulation with a mixture of hydrocarbons under fuel rich conditions, new chemistry was observed where the initiation reactions did not involve molecular oxygen as was the case for the oxidation of isolated hydrocarbons. For a mixture of methane, propene, *o*-xylene, and benzene, the initial reactions involved hydrocarbon decomposition or initiation by other radicals in the system. In addition, benzene was activated whereas benzene failed to react as an isolated hydrocarbon in an O_2 environment. The hydrocarbons were consumed by reaction with radicals produced during the simulation and started with the decomposition of propene. Because of the high concentration of hydrocarbon radicals, radical−radical recombination reactions were also observed. All of the reactions that have been reported were taken directly from analysis of the trajectory from the simulations. In ReaxFF, all possible reaction pathways are available; however, the simulations will follow the reaction pathways that are most kinetically and thermodynamically favorable. One could perform multiple simulations and analyze the trajectories to get a statistical distribution of the observed reactions to provide a measure of the importance of each pathway.

ReaxFF was also able to reproduce successfully the qualitative reaction rates with O_2 of benzene, methane, propene, and *o*-xylene, including the barrier heights of various reactions. ReaxFF can be used to calculate rate constants for combustion processes, but collecting sufficient statistics may require the study of numerous cases.

We consider these results as proof of concept that ReaxFF can be useful for elucidating the fundamental steps of complex reactions. Of course, a complete description of even these initial processes of combustion would require much longer simulations under conditions of lower temperature. With current computational resources, such simulations are quite manageable. Thus, it would be practical to use such ReaxFF simulations to calculate the rate constants of combustion reactions at various temperatures and pressures that could be extrapolated to experimental conditions. This could provide a valuable addition to mesoscale models of combustion and is an important step in understanding pre-ignition chemistry at the atomistic level.

Supporting Information Available: Description of the full ReaxFF potential functions, force field parameters described in this manuscript, and figures showing comparison between ReaxFF and QM energies for training set as well as a detailed reaction scheme for propene oxidation. This material is available free of charge via the Internet at http://pubs.acs.org.

References and Notes

(1) Simmie, J. M. *Prog. Energy Combust. Science* **2003**, *29*, 599.

(2) Gardiner, W. C., Jr.; Olson, D. B. *Ann. Rev. Phys. Chem.* **1980**, *31*, 377.

(3) Miller, J. A.; Kee, R. J.; Westbrook, C. K. *Ann. Rev. Phys. Chem.* **1990**, *41*, 345.

(4) Richter, H.; Howard, J. B. *Prog. Energ. Combust. Sci.* **2000**, *26*, 565.

(5) Miller, J. A. *Proc. Combust. Inst.* **1996**, *26*, 461.

(6) Cathonnet, M. *Combust. Sci. Tech.* **1994**, *98*, 265.

(7) Westbrook, C. K.; Mizobuchi, Y.; Poinset, T. J.; Smith, P. J.; Warnatz, J. *Proc. Combust. Inst.* **2005**, *30*, 125.

(8) Westbrook, C. K.; Dryer, F. L. *Prog. Energy Combust. Sci.* **1984**, *10*, 1.

(9) *Gas-Phase Combustion Chemistry*; Gardiner, W. C., Ed.; Springer-Verlag: New York, 2000.

(10) Qin, Z.; Lissianski, V. V.; Yang, H.; Gardiner, W. C.; Davis, S. G.; Wang, H. *Proc. Combust. Inst.* **2000**, *28*, 1663.

(11) Massias, A.; Diamantis, D.; Mastorakos, E.; Goussis, D. A. *Combust. Theory Model.* **1999**, *3*, 233.

(12) Sung, C. J.; Law, C. K.; Chen, J. Y. *Proc. Combust. Inst.* **2000**, *27*, 295.

(13) Blasenbrey, T.; Maas, U. *Proc. Combust. Inst.* **2000**, *28*, 1623.

(14) Taut, C.; Correa, C.; Deutschmann, O.; Warnatz, J.; Einecke, S.; Schulz, C.; Wolfrum, J. *Proc. Combust. Inst.* **2000**, *28*, 1153.

(15) Valorani, M.; Goussis, D. A. *J. Comp. Phys.* **2001**, *169*, 44.

(16) Mazyar, O. A.; Matheu, D. M.; Schwer, D. A.; Green, W. H., Jr. Preprints of *Symposia-ACS, Division of Fuel Chemistry* **2000**, *45*, 270.

(17) van Duin, A. C. T.; Dasgupta, S.; Lorant, F.; Goddard, W. A., III. *J. Phys. Chem. A* **2001**, *105*, 9396.

(18) Strachan, A.; van Duin, A. C. T.; Chakraborty, D.; Dasgupta, S.; Goddard, W. A., III. *Phys. Rev. Lett.* **2003**, *91*, 098301.

(19) Strachan, A.; Kober, E. M.; van Duin, A. C. T.; Oxgaard, J.; Goddard, W. A., III. *J. Chem. Phys.* **2005**, *122*, 054502.

(20) van Duin, A. C. T.; Zeiri, Y.; Dubnikova, F.; Kosloff, R.; Goddard, W. A., III. *J. Am. Chem. Soc.* **2005**, *127*, 11053.

(21) Chenoweth, K.; Cheung, S.; van Duin, A. C. T.; Goddard, W. A., III; Kober, E. M. *J. Am. Chem. Soc.* **2005**, *127*, 7192.

(22) Goddard, W. A., III; van Duin, A.; Chenoweth, K.; Cheng, M. J.; Pudar, S.; Oxgaard, J.; Merinov, B.; Jang, Y. H.; Persson, P. *Top. Catal.* **2006**, *38*, 93.

(23) Goddard, W. A., III; Merinov, B.; van Duin, A.; Jacob, T.; Blanco, M.; Molinero, V.; Jang, S. S.; Jang, Y. H. *Mol. Simul.* **2006**, *32* 251.

(24) Buehler, M. J.; van Duin, A. C. T.; Goddard, W. A., III. *Phys. Rev. Lett* **2006**, *96*, 095505.

(25) Ludwig, J.; Vlachos, D. G.; van Duin, A. C. T.; Goddard, W. A., III. *J. Phys. Chem. B* **2006**, *110*, 4274.

(26) Cheung, S.; Deng, W. Q.; van Duin, A. C. T.; Goddard, W. A., III. *J. Phys. Chem. A* **2006**, *109*, 851.

(27) Nielson, K. D.; van Duin, A. C. T.; Oxgaard, J.; Deng, W. Q.; Goddard, W. A., III. *J. Phys. Chem. A* **2005**, *109*, 493.

(28) Zhang, Q.; Cagin, T.; van Duin, A.; Goddard, W. A., III; Qi, Y.; Hector, L. G. *Phys. Rev. B* **2004**, *69*, 045423.

(29) Alwahabi, S. M.; Froment, G. F. *Ind. Eng. Chem. Res.* **2004**, *43*, 5098.

(30) Martens, G. G.; Marin, G. B.; Martens, J. A.; Jacobs, P. A.; Baron, G. V. *J. Catal.* **2006**, 195, 253.

(31) Martens, G. G.; Thybaut, J. W.; Marin, G. B. *Ind. Eng. Chem. Res.* **2001**, *40*, 1832.

(32) van Duin, A. C. T.; Baas, J. M. A.; van de Graaf, B. *J. Chem. Soc., Faraday Trans.* **1994**, *90*, 2881.

(33) Becke, A. D. *J. Chem. Phys.* **1993**, 98, 5648. Lee, C.; Yang, W.; Parr, R. G. *Phys. Rev. B* **1998**, 37, 785.

(34) Krishnan, R.; Binkley, J. S.; Seeger, R.; Pople, J. A. *J. Chem. Phys.* **1980**, *72*, 650.

(35) *Jaguar 6.5*; Schrodinger, LLC: Portland, OR, 2005.

(36) Curtiss, L. A.; Raghavachari, K.; Redfern, P. C.; Pople, J. A. *J. Chem. Phys.* **1997**, *106*, 1063.

(37) Xu, X.; Goddard, W. A., III. *PNAS* **2004**, *101*, 2673.

(38) Coote, M. L. *J. Phys. Chem. A* **2004**, *108*, 3865.

(39) Chakraborty, D.; Muller, R. P.; Dasgupta, S.; Goddard, W. A., III. *J. Phys. Chem. A* **2000**, *104*, 2261.

(40) Rogstad, K. N.; Jang, Y. H.; Sowers, L. C.; Goddard, W. A., III. *Chem. Res. Toxicol.* **2003**, *16*, 1455.

(41) Xu, X.; Muller, R. P.; Goddard, W. A., III. *PNAS* **2002**, 99, 3376.

(42) Feldmann, M. T.; Widicus, S. L.; Blake, G. A.; Kent, D. R., IV; Goddard, W. A., III. *J. Chem. Phys.* **2005**, *123*, 034304.

(43) Rudner, M. S.; Kent, IV, D. R.; Goddard, W. A., III; Roberts, J. D. *J. Phys. Chem. A* **2005**, *109*, 9083.

(44) Jang, Y. H.; Goddard, W. A., III. *J. Phys. Chem. B* **2006**, *110*, 7660.

(45) Baker, J.; Muir, M.; Andzelm, J.; Scheiner, A. In *Chemical Applications of Density Function Theory*; Laird, B. B., Ross, R. B., Ziegler, T., Eds.; ACS Symposium Series 629; American Chemical Society: Washington, DC, 1996.

(46) Niu, S. Q.; Hall, M. B. *Chem. Rev.* **2000**, *100*, 353.

(47) Oxgaard, J.; Periana, R. A.; Goddard, W. A., III. *J. Am. Chem. Soc.* **2004**, *126*, 11658.

(48) Benitez, D.; Goddard, W. A., III. *J. Am. Chem. Soc.* **2005**, *127*, 12218.

(49) Keith, J. M.; Nielsen, R. J.; Oxgaard, J.; Goddard, W. A., III. *J. Am. Chem. Soc.* **2005**, *127*, 13172.

(50) Jacob, T.; Goddard, W. A., III. *J. Phys. Chem. B* **2005**, *109*, 297.

(51) Keith, J. A.; Oxgaard, J.; Goddard, W. A., III. *J. Am. Chem. Soc.* **2006**, *128*, 3132.

(52) Ziatdinov, V. R.; Oxgaard, J.; Mironov, O. A.; Young, K. J. H.; Goddard, W. A., III; Periana, R. A. *J. Am. Chem. Soc.* **2006**, *128*, 7404.

(53) Nielsen, R. J.; Goddard, W. A., III. *J. Am. Chem. Soc.* **2006**, *128*, 9651.

(54) Oxgaard, J.; Bhalla, G.; Periana, R. A.; Goddard, W. A., III. *Organometallics* **2006**, *25*, 1618.

(55) Persson, P.; Lundqvist, M. J.; Ernstorfer, R.; Goddard, W. A., III; Willig, F. *J. Chem. Theory Comput.* **2006**, *2*, 441.

(56) Mortier, W. J.; Ghosh, K. S.; Shankar, S. J. *J. Am. Chem. Soc.* **1998**, *120*, 261.

(57) Hariharan, P. C.; Pople, J. A. *Theor. Chimica Acta* **1973**, *28*, 213. Francl, M. M.; Petro, W. J.; Hehre, W. J.; Binkley, J. S.; Gordon, M. S.; DeFrees, D. J.; Pople, J. A. *J. Chem. Phys.* **1982**, *77*, 3654.

(58) Berendsen, H. J. C.; Postma, J. P. M.; van Gunsteren, W. F.; DiNola, A.; Haak, J. R. *J. Chem. Phys. B* **1984**, *81*, 3684.

(59) Bourasseau, E.; Maillet, J.-B.; Mondelain, L.; Anglade, P.-M. *Mol. Simul.* **2005**, *31* 705.

(60) Yetter, R. A.; Rabitz, H.; Dryer, F. L.; Maki, R. G.; Klemm, R. B. *J. Chem. Phys.* **1989**, *91*, 4088.

(61) Sivakumaran, V.; Holscher, D.; Dillon, T. J.; Crowley, J. N. *Phys. Chem. Chem. Phys.* **2003**, *5*, 4821.

(62) Vasudevan, V.; Davidson, D. F.; Hanson, R. K. *Int. J. Chem. Kinet.* **2005**, *37*, 98.

(63) Xu, S.; Zhu, R. S.; Lin, M. C. *Int. J. Chem. Kinet.* **2006**, *38*, 322.

(64) De Joannon, M.; Sabia, P.; Tregrossi, A.; Cavaliere, A. *Combust. Sci. Tech.* **2004**, *176*, 769.

(65) Hidaka, Y.; Sato, K.; Henmi, Y.; Tanaka, H.; Inami, K. *Combust. Flame* **1999**, *118*, 340.

(66) Petersen, E. L.; Davidson, D. F.; Hanson, R. K. *Combust. Flame* **1999**, *117*, 272.

MD Simulations of Hydrocarbon Oxidation

J. Phys. Chem. A, Vol. 112, No. 5, 2008 **1053**

(67) Wilk, R. D.; Cernansky, N. P.; Cohen, R. S. *Combust. Sci. Tech.* **1987**, *52*, 39.

(68) Wilk, R. D.; Cernansky, N. P.; Pitz, W. J.; Westbrook, C. K. *Combust. Flame* **1989**, *77*, 145.

(69) Dagaut, P.; Cathonnet, M.; Boettner, J. C. *Combust. Sci. Tech.* **1992**, *83*, 167.

(70) Burcat, A.; Radhakrishnan, K. *Combust. Flame* **1985**, *60*, 157.

(71) Dagaut, P.; Cathonnet, M.; Boettner, J. C. *J. Phys. Chem.* **1988**, *92*, 661.

(72) Emdee, J. L.; Brezinsky, K.; Glassman, I. *Symp. (Int.) Combust.* **1990**, *23*, 77.

(73) Blanksby, S. J.; Ellison, G. B. *Acc. Chem. Res.* **2003**, *36*, 255.

(74) Thomas, S. D.; Bhargava, A.; Westmoreland, P. R.; Lindstedt, R. P.; Skevis, G. *Bull. Soc. Chim. Belg.* **1996**, *105*, 501.